Degradation of phonons in disordered moiré superlattices

Héctor Ochoa[1,2,3] and Rafael M. Fernandes[4]

[1]*Donostia International Physics Center, 20018 Donostia-San Sebastian, Spain*
[2]*IKERBASQUE, Basque Foundation for Science, Maria Diaz de Haro 3, 48013 Bilbao, Spain*
[3]*Department of Physics, Columbia University, New York, NY 10027, USA*
[4]*School of Physics and Astronomy, University of Minnesota, Minneapolis, MN 55455, USA*

The elastic collective modes of a moiré superlattice arise not from vibrations of a rigid crystal but from the relative displacement between the constituent layers. Despite their similarity to acoustic phonons, these modes, called phasons, are not protected by any conservation law. Here, we show that disorder in the relative orientation between the layers and thermal fluctuations associated with their sliding motion degrade the propagation of sound in the moiré superlattice. Specifically, the phason modes become overdamped at low energies and acquire a finite gap, which displays a universal dependence on the twist-angle variance. Thus, twist-angle inhomogeneity is manifested not only in the non-interacting electronic structure of moiré systems, but also in their phonon-like modes. More broadly, our results have important implications for the electronic properties of twisted moiré systems that are sensitive to the electron-phonon coupling.

Introduction. The discovery of twisted moiré systems has opened a new route to investigate correlated-electron and topological effects in highly-tunable narrow bands [1], both experimentally [2–14] and theoretically [15–58]. In the case of twisted bilayer graphene (TBG), several works have proposed that the electron-phonon interaction plays an important role in shaping the phase diagram, either by acting in tandem with strong electron-electron correlations or by possibly driving instabilities on its own, such as superconductivity [59–65]. Recent experiments in double-gated devices report superconductivity even when the Coulomb interaction is strongly screened [66–68], which might be an indication of electron-phonon coupling playing a prominent role in the emergence of superconductivity. Progress in this problem thus requires the elucidation of the lattice excitations at the energy and length scales of the moiré superlattice. While they are inherited from the phonon modes of the individual graphene layers, a full description is complicated by the adhesion forces between them and by the intrisic inhomogeneities of the relative displacement (heterostrain) and relative orientation (twist angle) of the layers.

To capture the low-energy electronic properties of TBG, one often considers electronic states that live on the sites and bonds of the triangular moiré superlattice (or of its dual) [69–73]. Analogously, to describe the low-energy phonons, it is convenient to focus on the collective excitations of the moiré lattice itself [74, 75], rather than on the lattice vibrations of the individual graphene layers. We focus on the in-plane motion as flexural modes are not expected to be very different than in monolayer graphene [74]. Importantly, the moiré pattern is a six-fold symmetric incommensurate superlattice, and not a rigid crystal. As a result, its low-energy elastic excitations are not described by acoustic phonons, but by so-called phasons [75, 76] – similarly to quasicrystals (see also [77]). The crucial difference is that while the dispersion of acoustic phonons is governed by the conservation of linear momentum of the ions of a rigid lattice, phasons in TBG are related to the relative translation between the layers, which is not a symmetry of the system since the layers are subjected to adhesion forces.

In this paper, we show that the phasons' dispersion is qualitatively altered by disorder and by anharmonic vibrations of the underlying graphene layers. In particular, we show that random forces affecting the relative orientation and displacement between the layers, no matter how small they are, give rise to a characteristic length scale L_c beyond which stacking order is lost. Thus, L_c, which depends on the elastic constants of graphene and on the strength of the disorder potentials, is the length scale associated with twist-angle inhomogeneity. Experimentally, inhomogeneous twist angles have been widely observed in TBG devices [78–80], and shown to strongly affect the electronic properties (see also [81, 82]). Within a region of size L_c, the distribution of twist angles θ has a variance:

$$\frac{\overline{\delta\theta^2}}{\overline{\theta}^2} \sim \frac{L_\mathrm{m}^2}{\pi^2 L_c^2} \ln\left(\frac{L_c}{L_\mathrm{m}}\right), \tag{1}$$

where the bar denotes disorder average, $\overline{\mathcal{O}} \equiv \langle \mathcal{O} \rangle_\mathrm{dis}$, $\delta\theta \equiv \theta - \overline{\theta}$, and L_m is the period of the moiré pattern. Thus, while for a twist angle variation of 1%, $L_c \gg L_\mathrm{m}$, for variations of 10%, $L_c \gtrsim L_\mathrm{m}$.

The twist-angle inhomogeneity scale L_c also gaps out the phason dispersion, introducing a new relevant energy scale of the order of $\delta\omega \sim \omega_\mathrm{ZB} L_\mathrm{m}/L_c$, where ω_ZB is the acoustic phonon frequency at the moiré Brillouin zone boundary. Combining with Eq. (1), we find an implicit and universal relationship between the twist angle variance and the phason-dispersion gap. Thus, twist angle inhomogeneity is not only manifested in the non-interacting electronic structure, but also in the low-energy elastic properties of TBG.

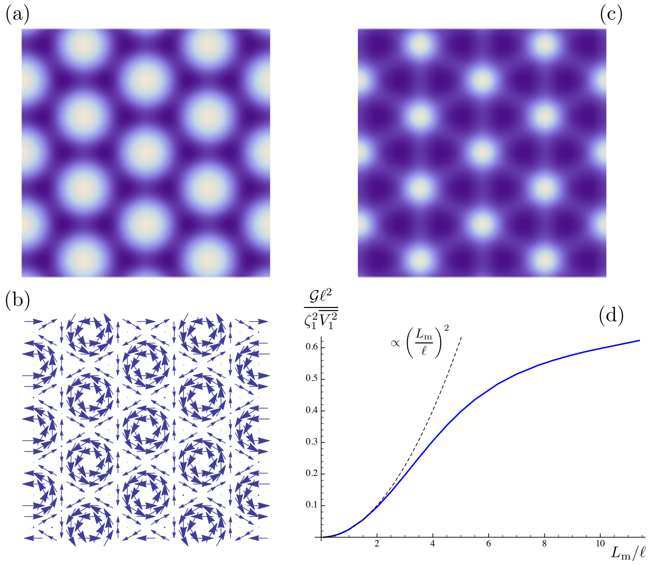

FIG. 1. **Stacking texture and disorder strength**. (a) Amplitude of the mass density wave generated by a rigid rotation of the layers. Bright spots correspond to areas of large overlap (AA-like stacking), dark areas are AB/BA minima. (b) Displacement field $\boldsymbol{u}_0(\mathbf{r})$ for $\bar{\theta} = 1.05^\mathrm{o}$. (c) The same as in (a), but now including the lattice relaxation in (b). (d) Long-wavelength limit of twist-angle disorder correlator $\mathscr{G}$ as a function of $L_\mathrm{m}/\ell \propto \overline{\theta}^{-1}$.

A gap opening in the phasons' dispersion is consistent with the fact that they are not protected by an underlying conservation law. For the same reason, the phasons' low-energy propagating dynamics is not robust either. Here, we demonstrate that anharmonic excitations introduce a damping term for the phason modes that does not vanish in the long-wavelength limit. Consequently, the phasons dynamics changes from propagating to diffusive. The typical scattering rate τ^{-1} increases substantially for decreasing twist angle as $\tau \sim \overline{\theta}^3$, highlighting the importance of this effect for small twist angles.

Stacking order and stacking susceptibility. Starting from a local, continuum approximation, the TBG interlayer tunneling Hamiltonian is given by [83, 84],

$$\hat{H}_\mathrm{inter} = \sum_{\zeta=\pm 1} \int d\mathbf{r}\, \hat{\psi}^\dagger_{\zeta,\mathrm{t}}(\mathbf{r})\, \hat{T}_\zeta(\mathbf{r})\, \hat{\psi}_{\zeta,\mathrm{b}}(\mathbf{r}) + \mathrm{h.c.} \tag{2}$$

Here $\hat{\psi}_{\zeta,\mathrm{b(t)}}$ is a Dirac spinor field defined in the sublattice space of bottom (top) layer around valleys $\mathbf{K}_\zeta = \zeta\,\mathbf{K}_+$ labelled by the chirality index $\zeta = \pm 1$. $\mathbf{K}_+ = (\boldsymbol{g}_1 - \boldsymbol{g}_2)/3$ is located at one of the corners of graphene's Brillouin zone, with $\boldsymbol{g}_{1,2}$ denoting the primitive vectors of the reciprocal lattice. The local tunneling matrix is

$$\hat{T}_\zeta(\mathbf{r}) = \sum_{n=0}^{2} e^{i\zeta(\mathbf{q}_n + \mathbf{K}_+)\cdot\boldsymbol{\phi}(\mathbf{r})}\, e^{i\zeta\frac{2\pi n}{3}\hat{\sigma}_z}\, \hat{\mathrm{T}}_\zeta\, e^{-i\zeta\frac{2\pi n}{3}\hat{\sigma}_z}, \tag{3}$$

where $\mathbf{q}_{0,1,2} = \mathbf{0}, \boldsymbol{g}_2, -\boldsymbol{g}_1$ are momentum transfers between equivalent Dirac points [83, 84], and $\hat{\mathrm{T}}_\zeta = w_\mathrm{AA}\,\hat{1} + w_\mathrm{AB}\,\hat{\sigma}_x$ contains the inter-layer tunneling amplitude w_AA (w_AB) involving the same (opposite) sublattices. In this equation, $\boldsymbol{\phi}(\mathbf{r})$ describes the spatial modulation of the pattern resulting from the overlap between the two layers (see Supplemental Material [85]):

$$\boldsymbol{\phi}(\mathbf{r}) = 2\sin\frac{\theta}{2}\,\hat{\mathbf{z}}\times\mathbf{r} + \boldsymbol{u}_0(\mathbf{r}) + \delta\boldsymbol{\phi}(\mathbf{r}). \tag{4}$$

Hereafter, we dub it the local *stacking order* function. If $\boldsymbol{\phi} = 0$, one would obtain a uniform AA stacking configuration and no moiré pattern. It is the twist angle θ, which appears in the first term of the equation above, that yields a sixfold symmetric moiré pattern with alternating AA and AB/BA stacking regions, as illustrated in Fig. 1 (a) (light and dark areas, respectively). However, this term corresponds to a rigid rotation between the layers, which in practice is never realized due to the non-negligible adhesion potential between the layers. For a nominal twist angle $\theta \to \overline{\theta}$, the free energy is minimized by a relative displacement between the layers, $\boldsymbol{u}_0(\mathbf{r})$. It is shown in Fig. 1 (b) for a relaxed structure around the magic angle, $\overline{\theta} = 1.05^\mathrm{o}$, yielding the moiré pattern of Fig. 1 (c) [85] (see also Refs. 86–88). Note that by keeping a non-zero $\overline{\theta}$ we are implicitly incorporating the action of lateral forces needed to stabilize the moiré pattern over the Bernal stacking. Determining the origin of these lateral forces require first-principles calculations that are beyond the scope of this work [89]. The main focus of this Letter is the last term in Eq. (4), $\delta\boldsymbol{\phi}(\mathbf{r})$, which describes local stacking deviations around the local minimum of the mechanical energy.

Mechanical forces acting on the layers will naturally give rise to a finite stacking deviation $\delta\boldsymbol{\phi}(\mathbf{r})$. These forces can be extrinsic (e.g. applied strain) or intrinsic (e.g. due to random strain or thermal fluctuations). They are generically described by a function $\boldsymbol{f}(\mathbf{r})$, which in turn can be decomposed into a relative stress and a relative torque between the layers, causing changes in their relative displacement and orientation, respectively. In frequency domain, the stacking deviation caused by such a force is given by

$$\delta\boldsymbol{\phi}(\mathbf{r},\omega) = \int d^2\mathbf{r}'\ \hat{\chi}_0(\mathbf{r},\mathbf{r}',\omega)\cdot\boldsymbol{f}(\mathbf{r}',\omega). \tag{5}$$

where we introduced the dynamic stacking susceptibility tensor $\hat{\chi}_0(\mathbf{r},\mathbf{r}',\omega)$.

We first focus on the static case. Due to the (approximate) translational symmetry of the moiré superlattice, the stacking susceptibility can be parametrized in momentum space as $\chi_{0,(i,j);(\mathbf{G}_1,\mathbf{G}_2)}(\mathbf{q})$, with $\mathbf{q}$ restricted to the moiré Brillouin zone and $\mathbf{G}_i = -2\sin\frac{\overline{\theta}}{2}\,\hat{\mathbf{z}}\times\boldsymbol{g}_i$ the vectors of the moiré reciprocal lattice. One can directly compute it from the "mechanical" free-energy functional of TBG, which includes the intrinsic elastic contributions from the individual layers and the adhesion potential $\mathscr{V}_{\mathrm{ad}}$ between them. We obtain [85]:

$$\left[\hat{\chi}_0^{-1}(\mathbf{q})\right]_{i,j;\mathbf{G}_1,\mathbf{G}_2} = \frac{\lambda+\mu}{2}\left(\mathbf{q}+\mathbf{G}_1\right)_i\left(\mathbf{q}+\mathbf{G}_2\right)_j\delta_{\mathbf{G}_1,\mathbf{G}_2} + \frac{\mu}{2}\left(\mathbf{q}+\mathbf{G}_1\right)\cdot\left(\mathbf{q}+\mathbf{G}_2\right)\delta_{ij}\delta_{\mathbf{G}_1,\mathbf{G}_2} + \mathscr{V}_{ij}^{(2)}\left(\mathbf{G}_2-\mathbf{G}_1\right), \quad (6)$$

where $\mu = 9.57$ eV/Å^2 and $\lambda \approx 3.25$ eV/Å^2 are graphene's Lamé coefficients [90] and $\mathscr{V}_{ij}^{(2)}(\mathbf{G})$ are the Fourier components of the harmonic expansion of the adhesion potential $\mathscr{V}_{\mathrm{ad}}$,

$$\mathscr{V}_{\mathrm{ad}}(\boldsymbol{\phi}) = \frac{V_{\mathrm{AA}}}{3} + \frac{2V_{\mathrm{AA}}}{9}\sum_{i=1}^{3}\cos\left(\boldsymbol{g}_i\cdot\boldsymbol{\phi}\right), \quad (7)$$

where $\boldsymbol{g}_3 = -\boldsymbol{g}_1 - \boldsymbol{g}_2$. The key quantity here is $V_{\mathrm{AA}} \approx 4$ meV/Å^2 [91], which is the free energy difference between AA and AB/BA stacking configurations.

Diagonalization of Eq. (6) determines the spectrum of harmonic oscillations around the minimum energy configuration, $\boldsymbol{\phi}_0(\mathbf{r}) = 2\sin\frac{\overline{\theta}}{2}\,\hat{\mathbf{z}}\times\mathbf{r} + \boldsymbol{u}_0(\mathbf{r})$, which is controlled by the ratio of the two length scales in the problem: the moiré pitch $L_{\mathrm{m}} = a/(2\sin\frac{\overline{\theta}}{2})$ and the characteristic width of stacking domain walls connecting degenerate AB and BA minima (dark regions in Fig. 1c),

$$\ell = \frac{3a}{4\pi}\sqrt{\frac{\mu}{V_{\mathrm{AA}}}} \approx 3\,\mathrm{nm}. \quad (8)$$

The ratio $L_{\mathrm{m}}/\ell \propto \overline{\theta}^{-1}$ characterizes the amount of lattice relaxation, i.e., how sharp $\boldsymbol{\phi}_0(\mathbf{r})$ is on the moiré scale. The spectral decomposition of the stacking susceptibility then reads

$$\hat{\chi}_0(\mathbf{q}) = 2\sum_n \frac{\hat{\boldsymbol{e}}_n(\mathbf{q})\otimes\hat{\boldsymbol{e}}_n^{\dagger}(\mathbf{q})}{\varrho\,\omega_n^2(\mathbf{q})}, \quad (9)$$

where $\varrho \approx 7.6\times10^{-7}$ kg/m^2 is graphene's mass density and $\omega_n(\mathbf{q})$, $\hat{\boldsymbol{e}}_n(\mathbf{q}) = \sum_{i,\mathbf{G}} c_{i,\mathbf{G}}^n(\mathbf{q})\,\hat{\boldsymbol{e}}_{i,\mathbf{G}}$ are the dispersion and the polarization vector of vibrational mode n of the moiré pattern, respectively. In the long-wavelength and low-energy limit, one obtains two acoustic-like longitudinal and transverse modes, $\omega_{L,T} = c_{L,T}|\mathbf{q}|$ [74–76]. These so-called phasons are associated with the invariance of the *equilibrium* free energy with respect to a uniform translation $\tilde{\boldsymbol{u}}$ of the center of the stacking texture, $\boldsymbol{\phi}_0(\mathbf{r}) \to \boldsymbol{\phi}_0(\mathbf{r}-\tilde{\boldsymbol{u}})$. In the limit of vanishing adhesion forces and small twist angles, the latter can be written in terms of the relative displacement between the layers as $\tilde{\boldsymbol{u}} = \overline{\theta}^{-1}\hat{\mathbf{z}}\times(\boldsymbol{u}_{\mathrm{t}}-\boldsymbol{u}_{\mathrm{b}})$; however, the general relationship between them is more complicated. Note also that longitudinal phason fluctuations (of the collective coordinate $\tilde{\boldsymbol{u}}$) involve transverse stacking fluctuations, and viceversa; hereafter the indices L,T refer to the latter. The sound velocities $c_{L,T}$ are only slightly smaller than for the corresponding acoustic phonons of monolayer graphene, as the lower stiffness of the stacking domains walls is compensated by the smaller inertia of the sliding motion [74, 75].

Static response: disorder effects. We first investigate the impact of quenched disorder on the phason modes. The most relevant types of disorder that affect the moiré pattern (i.e. the stacking order) are those that locally change the relative orientation (twist angle) as well as the relative displacement (heterostrain) between the layers. The corresponding disorder potentials can be parametrized, respectively, in terms of a random layer-symmetric potential $V_1(\mathbf{r})$ and a random layer asymmetric potential $V_2(\mathbf{r})$, which give rise to forces of the form:

$$\boldsymbol{f}(\mathbf{r}) = -\left(\hat{\boldsymbol{z}}\times\boldsymbol{\nabla}\right)V_1(\mathbf{r}) - \boldsymbol{\nabla}V_2(\mathbf{r}). \quad (10)$$

The disorder-averaged correlation function between local stacking configurations, $C_{ij} = \langle\delta\phi_i(\mathbf{r})\delta\phi_j(\mathbf{r}')\rangle_{\mathrm{dis}}$, is given in linear response by

$$\hat{C}(\mathbf{r},\mathbf{r}') = \int d^2\mathbf{r}_1\int d^2\mathbf{r}_2\;\hat{\chi}_0(\mathbf{r},\mathbf{r}_1)\cdot\hat{\mathscr{G}}(\mathbf{r}_1,\mathbf{r}_2)\cdot\hat{\chi}_0(\mathbf{r}_2,\mathbf{r}'), \quad (11)$$

where

$$\mathscr{G}_{ij}(\mathbf{r}_1,\mathbf{r}_2) \equiv \left\langle f_i(\mathbf{r}_1)\,f_j(\mathbf{r}_2)\right\rangle_{\mathrm{dis}}. \quad (12)$$

Note that the correlation function $\hat{C}$ is related to the (renormalized) susceptibility $\hat{\chi}$ via the fluctuation-dissipation theorem. To proceed, we assume that the disorder potentials V_α are smooth on the inter-atomic scale and decay on a characteristic length scale $\zeta_\alpha \ll L_{\mathrm{m}}$. Moreover, we consider them to follow random Gaussian distributions with $\overline{V_\alpha} = 0$ and finite $\overline{V_\alpha^2}$.

To determine how disorder affects the stacking order and the vibrational modes, Eq. (9), we project the averaged force on the subspace of the low-energy phason modes $n_{1,2} = L,T$, $\mathscr{G}_{n_1,n_2}(\mathbf{q}) = \hat{\boldsymbol{e}}_{n_1}^{\dagger}(\mathbf{q})\cdot\hat{\mathscr{G}}(\mathbf{q})\cdot\hat{\boldsymbol{e}}_{n_2}(\mathbf{q})$. Its long-wavelength behavior depends crucially on the adhesion potential $\mathscr{V}_{\mathrm{ad}}$ that couples the two layers, Eq. (7). If $V_{\mathrm{AA}} = 0$, the system would be invariant under relative translations of the layers, leading to $\mathscr{G}_{n_1,n_2}(\mathbf{q}) \sim |\mathbf{q}|^2$. As a result, from Eq. (11), since $\hat{\chi}_0^{-1} \sim |\mathbf{q}|^2$, $\hat{C}(\mathbf{q})$ would diverge only as $\sim|\mathbf{q}|^{-2}$, implying quasi-long-range stacking order [85]. However, once $V_{\mathrm{AA}} > 0$, as in TBG, relative translations of the layers are no longer a symmetry, and we obtain $\mathscr{G}_{n_1,n_2}(\mathbf{q}\to\mathbf{0}) = \mathscr{G}\,\delta_{n_1,n_2}$ [85]. Consequently, $\hat{C}(\mathbf{q})$ now diverges as $\sim |\mathbf{q}|^{-4}$, which implies loss of stacking order, in agreement with the Imry-Ma criterion [92]. More specifically, stacking correlations in the relaxed moiré structure decay exponentially [85],

$$\left\langle e^{i\boldsymbol{g}\cdot\left(\delta\boldsymbol{\phi}(\mathbf{r})-\delta\boldsymbol{\phi}(\mathbf{r}')\right)}\right\rangle_{\rm dis} \sim \left(\frac{L}{|\mathbf{r}-\mathbf{r}'|}\right)^{-\frac{|\mathbf{r}-\mathbf{r}'|^2}{2L_c^2}}, \qquad (13)$$

where L is the size of the system and L_c is the characteristic length scale beyond which the moiré pattern ceases to respond elastically to external forces,

$$L_c = \frac{a\varrho}{\sqrt{4\pi\mathscr{G}}}\frac{c_L^2 c_T^2}{\sqrt{c_L^4+c_T^4}}. \qquad (14)$$

This result follows from the first cumulant approximation for the correlator in Eq. (13), where the fast growth of $C(\mathbf{x},\mathbf{y})$ with the relative distance gives rise to an exponential suppression of stacking order. The characteristic scale of this decay reflects the competition between the stiffness of the moiré pattern and the accumulated action of disorder forces on the stacking texture. Equation (1) for the twist-angle variation inside a region of length L_c is obtained by computing the fluctuations of $\delta\theta = (\boldsymbol{\nabla}\times\delta\boldsymbol{\phi})_z$ cut-off by L_c [85]. We emphasize that this last result does not depend on the form of the disorder potentials, but rather on the presence of interlayer adhesion forces.

Upon computing the "disorder strength" $\mathscr{G}$, we find that the contribution from the potential V_1 (associated with twist angle disorder) is several orders of magnitude larger than that from V_2 (associated with heterostrain disorder). The reason is that the relaxed structure generates very little longitudinal strain in order to preserve the symmetry of the moiré pattern. Thus, we associate L_c with the length-scale of twist-angle inhomogeneity. Fig. 1 (d) shows a numerical evaluation of $\mathscr{G}$ as a function of $L_{\rm m}/\ell \propto \overline{\theta}^{-1}$ [85]. While $\mathscr{G}$ increases quadratically with $L_{\rm m}/\ell$ in the region of large twist angles, it seems to saturate to an angle-independent value for large $L_{\rm m}/\ell$, $L_c \sim a\mu\ell/\zeta_1(\overline{V_1^2})^{1/2}$, which can be interpreted as a collective pinning length of the stacking domain wall system, akin to the case of an incommensurate charge density wave [93].

Because stacking order is lost at the length scale L_c, the phasons acquire a gap at a momentum scale $q_c = 2\pi/L_c$ [Fig. 2(a)]. We can use the long-wavelength dispersion $\omega_n = c_n|\mathbf{q}|$ to estimate the gap $\delta\omega_n = \omega_{n,\rm ZB}L_{\rm m}/L_c$, where $\omega_{n,\rm ZB}$ is the extrapolated phonon frequency at the zone boundary $q_{\rm ZB} = 2\pi/L_{\rm m}$. Since the ratio $L_{\rm m}/L_c$ is an implicit function of the twist angle variance, Eq. (1), the relative phason gap is a universal function of $\overline{\delta\theta^2}/\overline{\theta}^2$, as illustrated in Fig. 2(a).

Dynamical response: anharmonic effects. While quenched disorder impacts the static properties of the stacking susceptibility, thermal fluctuations affect its dynamics. Indeed, the lack of a conservation law that protects the gapless dispersion of the phasons also leaves its propagating dynamics unprotected. Quite generally, the renormalized stacking susceptibility $\hat{\chi}$ can be parametrized as [94],

$$\hat{\chi}(\mathbf{q},\omega) = \left[\hat{\chi}_0^{-1}(\mathbf{q}) - \frac{\varrho}{2}\omega^2\hat{1} - i\omega\hat{\sigma}(\mathbf{q},\omega)\right]^{-1}, \qquad (15)$$

where $\hat{\chi}_0^{-1}$ is given by Eq. (6) and the memory matrix function $\hat{\sigma}(\mathbf{q},\omega)$ can be extracted from the imaginary part of the phason self-energy. Specifically, $\sigma_{n_1,n_2}(\mathbf{q},\omega)$ can be expressed as a thermal correlator of forces on the specific phason modes $n_{1,2}$ exerted by the other stacking degrees of freedom [85]. The most relevant type of thermal fluctuations in our model are those arising from anharmonic contributions in the adhesion potential of Eq. (7). Formally, these anharmonic terms induce a self-interaction for the stacking fluctuations and, consequently, dissipation.

The detailed computation of $\hat{\sigma}(\mathbf{q},\omega)$ projected onto the n_1, n_2 phason modes, $\sigma_{n_1,n_2}(\mathbf{q},\omega)$, is shown in the Supplemental Material [85]. In the absence of an adhesion potential (i.e. $V_{\rm AA}=0$), the linear momentum of each layer is locally conserved, and we find $\sigma_{n_1,n_2}(\mathbf{q},\omega) \propto |\mathbf{q}|^2$.

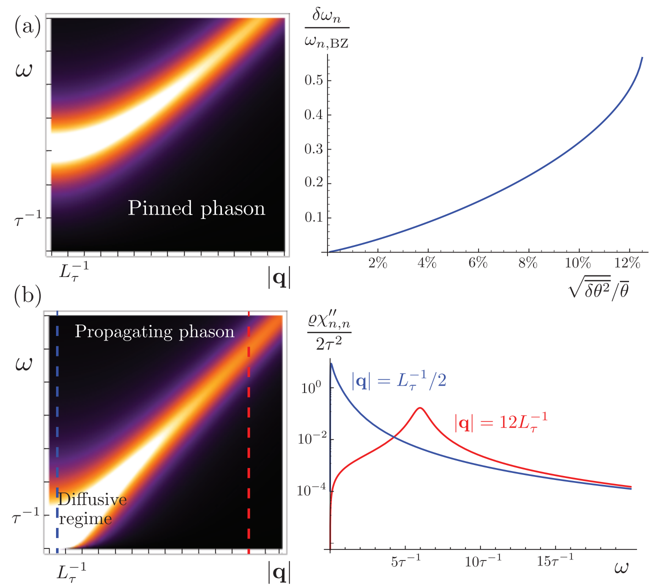

FIG. 2. **Phason dispersion relation**. (a) Density plot of the imaginary part of the stacking susceptibility, $\chi''_{n,n}$, in the presence of disorder ($L_c = L_\tau$). The right panel shows the evolution of the phason gap as a function of twist-angle disorder. (b) The same as in (a) in the absence of disorder. At long wavelengths, $|\mathbf{q}| < 1/L_\tau$, phasons are overdamped. The right panel shows constant momentum cuts in the diffusive (blue) and propagating (red) regimes, the latter characterized by a sharp quasiparticle peak (note that the vertical axis is in logarithmic scale).

In this case, the low-frequency phason modes display propagating dynamics, akin to the case of regular acoustic phonons. However, in the realistic case of a nonzero adhesion potential, $\sigma_{n_1,n_2}(\mathbf{q},\omega)$ remains finite in the long-wavelength limit $\mathbf{q}\to 0$, where $\tau^{-1}\equiv 2\sigma_{n,n}(0,0)/\varrho$ can then be identified as the relaxation rate of the relative momentum between the layers. This is determined by resonant processes in which thermally populated amplitude vibrations in mode n_i are converted into mode n_j via phason scattering conserving energy and quasi-momentum. At large angles, these processes are dominated by interlayer phonon umklapp in the moiré superlattice, leading to a quick growth with decreasing twist angle, $\tau^{-1}\propto(\overline{\theta})^{-3}$ [85]. The main consequence of a finite τ in Eq. (15) is that, for small momenta, $|\mathbf{q}|<1/L_\tau$, with $L_\tau = 2\tau c_n$, the dynamics of the phason modes becomes diffusive, $\omega_n(\mathbf{q})\approx -i\tau c_n^2|\mathbf{q}|^2$. This behavior is illustrated in Fig. 2(b).

Discussion. In this paper, we showed how deviations in the stacking order of the graphene layers in TBG fundamentally alter the elastic properties of the resulting moiré pattern. These stacking deviations are promoted either by disorder in the relative orientation (twist angle) and relative displacement (heterostrain) between the layers, or by thermally-excited anharmonic fluctuations of the lattice. In the presence of adhesion forces between the layers, the former introduce a length scale L_c beyond which the moiré pattern lacks positional order, while the latter generates a time scale τ beyond which the relative momentum between the layers relaxes. Whereas L_c has a monotonic dependence on the twist-angle variance, $\overline{\delta\theta^2}/\overline{\theta}^2$ [Eq. 1], τ is strongly suppressed for decreasing twist angles, $\tau\propto\overline{\theta}^3$. Both quantities qualitatively change the low-energy, long-wavelength excitations of the moiré superlattice. Instead of behaving like gapless propagating acoustic phonons, these phasons become gapped (due to finite L_c) and diffusive (due to finite τ). These are the consequences of the absence of a conservation law protecting these soft modes. Atomistic models for interfacial forces [89] can provide better numerical estimates and shed more light on the stability of moiré patterns.

Twist angle variations are manifested as local changes in the electronic density. Our work reveals a hitherto unexplored facet of this ubiquitous property of TBG devices, showing its crucial role in shaping the phason modes of the moiré superlattice. Indeed, the typical experimental values $\sqrt{\overline{\delta\theta^2}}\sim 0.02^o-0.04^\circ$ around the magic angle $\overline{\theta}\sim 1^\circ$ [78, 80] give $L_c\sim 400-200$ nm, which imply random pinning forces $\zeta_1(\overline{V_1^2})^{1/2}$ comparable to the surface tension of stacking domain walls ($\ell\, V_{\mathrm{AA}}\approx 1$ eV/nm) and a phason gap of $4\%-9\%$ of $\omega_{n,\mathrm{ZB}}\sim 40$ K. The phason dynamics should be manifested in thermodynamic properties at low temperatures, such as in the specific heat capacity [95, 96]. Importantly, via the electron-phonon coupling, the changes in the phason modes promoted by twist-angle variations – and anharmonic forces – will inevitably impact the electronic properties in different ways. This includes the renormalized dispersion of the remote and narrow bands [46, 97], the contribution to the resistivity arising from electron-phonon scattering [61, 76, 98, 99], and the ordered states that can be either promoted or strongly affected by electron-phonon interactions, such as superconductivity [59–64] and nematicity [12, 65, 100].

H.O. acknowledges NSF MRSEC program Grant No. DMR-1420634. R.M.F. was supported by the U.S. Department of Energy, Office of Science, Basic Energy Sciences, Materials Science and Engineering Division, under Award No. DE-SC0020045.

[1] L. Balents, C. R. Dean, D. K. Efetov, and A. F. Young, Nat. Phys. **16**, 725 (2020).

[2] Y. Cao, V. Fatemi, S. Fang, K. Watanabe, T. Taniguchi, E. Kaxiras, and P. Jarillo-Herrero, Nature **556**, 43 (2018).

[3] Y. Cao, V. Fatemi, A. Demir, S. Fang, S. L. Tomarken, J. Y. Luo, J. D. Sanchez-Yamagishi, K. Watanabe, T. Taniguchi, E. Kaxiras, R. C. Ashoori, and P. Jarillo-Herrero, Nature **556**, 80 (2018).

[4] M. Yankowitz, S. Chen, H. Polshyn, Y. Zhang, K. Watanabe, T. Taniguchi, D. Graf, A. F. Young, and C. R. Dean, Science **363**, 1059 (2019).

[5] A. L. Sharpe, E. J. Fox, A. W. Barnard, J. Finney, K. Watanabe, T. Taniguchi, M. A. Kastner, and D. Goldhaber-Gordon, Science **365**, 605 (2019).

[6] Y. Jiang, X. Lai, K. Watanabe, T. Taniguchi, K. Haule, J. Mao, and E. Y. Andrei, Nature **573**, 91 (2019).

[7] A. Kerelsky, L. J. McGilly, D. M. Kennes, L. Xian, M. Yankowitz, S. Chen, K. Watanabe, T. Taniguchi, J. Hone, C. Dean, A. Rubio, and A. N. Pasupathy, Nature **572**, 95 (2019).

[8] X. Lu, P. Stepanov, W. Yang, M. Xie, M. A. Aamir, I. Das, C. Urgell, K. Watanabe, T. Taniguchi, G. Zhang, A. Bachtold, A. H. MacDonald, and D. K. Efetov, Nature **574**, 653 (2019).

[9] Y. Xie, B. Lian, B. Jäck, X. Liu, C.-L. Chiu, K. Watanabe, T. Taniguchi, B. A. Bernevig, and A. Yazdani, Nature **572**, 101 (2019).

[10] Y. Choi, J. Kemmer, Y. Peng, A. Thomson, H. Arora, R. Polski, Y. Zhang, H. Ren, J. Alicea, G. Refael, F. v. Oppen, K. Watanabe, T. Taniguchi, and S. Nadj-Perge, Nat. Phys. **15**, 1174 (2019).

[11] M. Serlin, C. Tschirhart, H. Polshyn, Y. Zhang, J. Zhu, K. Watanabe, T. Taniguchi, L. Balents, and A. Young, Science **367**, 900 (2020).

[12] Y. Cao, D. Rodan-Legrain, J. M. Park, N. F. Q. Yuan, K. Watanabe, T. Taniguchi, R. M. Fernandes, L. Fu, and P. Jarillo-Herrero, Science **372**, 264 (2021).

[13] A. Rozen, J. M. Park, U. Zondiner, Y. Cao, D. Rodan-Legrain, T. Taniguchi, K. Watanabe, Y. Oreg, A. Stern, E. Berg, *et al.*, Nature **592**, 214 (2021).

[14] Y. Saito, F. Yang, J. Ge, X. Liu, T. Taniguchi, K. Watanabe, J. Li, E. Berg, and A. F. Young, Na-

ture **592**, 220 (2021).
[15] C. Xu and L. Balents, Phys. Rev. Lett. **121**, 087001 (2018).
[16] H. C. Po, L. Zou, A. Vishwanath, and T. Senthil, Phys. Rev. X **8**, 031089 (2018).
[17] H. Isobe, N. F. Q. Yuan, and L. Fu, Phys. Rev. X **8**, 041041 (2018).
[18] D. M. Kennes, J. Lischner, and C. Karrasch, Phys. Rev. B **98**, 241407 (2018).
[19] L. Rademaker and P. Mellado, Phys. Rev. B **98**, 235158 (2018).
[20] J. F. Dodaro, S. A. Kivelson, Y. Schattner, X. Q. Sun, and C. Wang, Phys. Rev. B **98**, 075154 (2018).
[21] A. Thomson, S. Chatterjee, S. Sachdev, and M. S. Scheurer, Phys. Rev. B **98**, 075109 (2018).
[22] Y.-P. Lin and R. M. Nandkishore, Phys. Rev. B **98**, 214521 (2018).
[23] F. Guinea and N. R. Walet, Proc. Natl. Acad. Sci. U.S.A. **115**, 13174 (2018).
[24] Y. Sherkunov and J. J. Betouras, Phys. Rev. B **98**, 205151 (2018).
[25] C.-C. Liu, L.-D. Zhang, W.-Q. Chen, and F. Yang, Phys. Rev. Lett. **121**, 217001 (2018).
[26] J. W. F. Venderbos and R. M. Fernandes, Phys. Rev. B **98**, 245103 (2018).
[27] Z. Song, Z. Wang, W. Shi, G. Li, C. Fang, and B. A. Bernevig, Phys. Rev. Lett. **123**, 036401 (2019).
[28] J. Kang and O. Vafek, Phys. Rev. Lett. **122**, 246401 (2019).
[29] J. M. Pizarro, M. J. Calderón, and E. Bascones, J. Phys. Commun. **3**, 035024 (2019).
[30] G. Tarnopolsky, A. J. Kruchkov, and A. Vishwanath, Phys. Rev. Lett. **122**, 106405 (2019).
[31] B. Roy and V. Juricic, Phys. Rev. B **99**, 121407 (2019).
[32] Y.-P. Lin and R. M. Nandkishore, Phys. Rev. B **100**, 085136 (2019).
[33] K. Hejazi, C. Liu, H. Shapourian, X. Chen, and L. Balents, Phys. Rev. B **99**, 035111 (2019).
[34] T. Huang, L. Zhang, and T. Ma, Sci. Bull. **64**, 310 (2019).
[35] Y.-H. Zhang, D. Mao, Y. Cao, P. Jarillo-Herrero, and T. Senthil, Phys. Rev. B **99**, 075127 (2019).
[36] J. González and T. Stauber, Phys. Rev. Lett. **122**, 026801 (2019).
[37] L. Classen, C. Honerkamp, and M. M. Scherer, Phys. Rev. B **99**, 195120 (2019).
[38] K. Seo, V. N. Kotov, and B. Uchoa, Phys. Rev. Lett. **122**, 246402 (2019).
[39] N. F. Yuan, H. Isobe, and L. Fu, Nature Communications **10**, 5769 (2019).
[40] J. Kang and O. Vafek, Phys. Rev. B **102**, 035161 (2020).
[41] M. Xie and A. H. MacDonald, Phys. Rev. Lett. **124**, 097601 (2020).
[42] C. Repellin, Z. Dong, Y.-H. Zhang, and T. Senthil, Phys. Rev. Lett. **124**, 187601 (2020).
[43] Y. Xu, X.-C. Wu, C.-M. Jian, and C. Xu, Phys. Rev. B **101**, 205426 (2020).
[44] M. Christos, S. Sachdev, and M. S. Scheurer, Proc. Natl. Acad. Sci. U.S.A. **117**, 29543 (2020).
[45] N. Bultinck, E. Khalaf, S. Liu, S. Chatterjee, A. Vishwanath, and M. P. Zaletel, Phys. Rev. X **10**, 031034 (2020).
[46] O. Vafek and J. Kang, Phys. Rev. Lett. **125**, 257602 (2020).
[47] Y. Zhang, K. Jiang, Z. Wang, and F. Zhang, Phys. Rev. B **102**, 035136 (2020).
[48] T. Cea and F. Guinea, Phys. Rev. B **102**, 045107 (2020).
[49] E. Brillaux, D. Carpentier, A. A. Fedorenko, and L. Savary, arXiv:2008.05041 (2020).
[50] B. A. Bernevig, Z.-D. Song, N. Regnault, and B. Lian, Phys. Rev. B **103**, 205413 (2021).
[51] B. Lian, Z.-D. Song, N. Regnault, D. K. Efetov, A. Yazdani, and B. A. Bernevig, Phys. Rev. B **103**, 205414 (2021).
[52] F. Xie, A. Cowsik, Z.-D. Song, B. Lian, B. A. Bernevig, and N. Regnault, Phys. Rev. B **103**, 205416 (2021).
[53] Y. Da Liao, J. Kang, C. N. Breiø, X. Y. Xu, H.-Q. Wu, B. M. Andersen, R. M. Fernandes, and Z. Y. Meng, Phys. Rev. X **11**, 011014 (2021).
[54] Y. Wang, J. Kang, and R. M. Fernandes, Phys. Rev. B **103**, 024506 (2021).
[55] P. Potasz, M. Xie, and A. H. MacDonald, arXiv:2102.02256 (2021).
[56] E. Khalaf, S. Chatterjee, N. Bultinck, M. P. Zaletel, and A. Vishwanath, Science Advances **7** (2021), 10.1126/sciadv.abf5299.
[57] J. Kang, B. A. Bernevig, and O. Vafek, arXiv:2104.01145 (2021).
[58] D. V. Chichinadze, L. Classen, Y. Wang, and A. V. Chubukov, arXiv:2108.05334 (2021).
[59] F. Wu, A. H. MacDonald, and I. Martin, Phys. Rev. Lett. **121**, 257001 (2018).
[60] B. Lian, Z. Wang, and B. A. Bernevig, Phys. Rev. Lett. **122**, 257002 (2019).
[61] F. Wu, E. Hwang, and S. Das Sarma, Phys. Rev. B **99**, 165112 (2019).
[62] M. Angeli, E. Tosatti, and M. Fabrizio, Phys. Rev. X **9**, 041010 (2019).
[63] C. Lewandowski, D. Chowdhury, and J. Ruhman, Phys. Rev. B **103**, 235401 (2021).
[64] T. Cea and F. Guinea, arXiv:2103.01815 (2021).
[65] R. M. Fernandes and J. W. F. Venderbos, Science Advances **6**, eaba8834 (2020).
[66] P. Stepanov, I. Das, X. Lu, A. Fahimniya, K. Watanabe, T. Taniguchi, F. H. L. Koppens, J. Lischner, L. Levitov, and D. K. Efetov, Nature **583**, 375 (2020).
[67] Y. Saito, J. Ge, K. Watanabe, T. Taniguchi, and A. F. Young, Nat. Phys. **16**, 926 (2020).
[68] X. Liu, Z. Wang, K. Watanabe, T. Taniguchi, O. Vafek, and J. I. A. Li, Science **371**, 1261 (2021).
[69] M. Koshino, N. F. Q. Yuan, T. Koretsune, M. Ochi, K. Kuroki, and L. Fu, Phys. Rev. X **8**, 031087 (2018).
[70] J. Kang and O. Vafek, Phys. Rev. X **8**, 031088 (2018).
[71] N. F. Q. Yuan and L. Fu, Phys. Rev. B **98**, 045103 (2018).
[72] L. Zou, H. C. Po, A. Vishwanath, and T. Senthil, Phys. Rev. B **98**, 085435 (2018).
[73] H. C. Po, L. Zou, T. Senthil, and A. Vishwanath, Phys. Rev. B **99**, 195455 (2019).
[74] M. Koshino and Y.-W. Son, Phys. Rev. B **100**, 075416 (2019).
[75] H. Ochoa, Phys. Rev. B **100**, 155426 (2019).
[76] I. Maity, M. H. Naik, P. K. Maiti, H. R. Krishnamurthy, and M. Jain, Phys. Rev. Res. **2**, 013335 (2020).
[77] J. Gaa, G. Palle, R. M. Fernandes, and J. Schmalian, Phys. Rev. B **104**, 064109 (2021).
[78] A. Uri, S. Grover, Y. Cao, J. Crosse, K. Bagani, D. Rodan-Legrain, Y. Myasoedov, K. Watanabe,

T. Taniguchi, P. Moon, M. Koshino, P. Jarillo-Herrero, and E. Zeldov, Nature **581**, 47 (2020).

[79] T. Benschop, T. A. de Jong, P. Stepanov, X. Lu, V. Stalman, S. J. van der Molen, D. K. Efetov, and M. P. Allan, Phys. Rev. Research **3**, 013153 (2021).

[80] N. P. Kazmierczak, M. Van Winkle, C. Ophus, K. C. Bustillo, S. Carr, H. G. Brown, J. Ciston, T. Taniguchi, K. Watanabe, and D. K. Bediako, Nature Materials (2021).

[81] J. H. Wilson, Y. Fu, S. Das Sarma, and J. H. Pixley, Phys. Rev. Research **2**, 023325 (2020).

[82] B. Padhi, A. Tiwari, T. Neupert, and S. Ryu, Phys. Rev. Research **2**, 033458 (2020).

[83] J. M. B. L. dos Santos, N. M. R. Peres, and A. H. C. Neto, Phys. Rev. Lett. **99**, 256802 (2007).

[84] R. Bistritzer and A. H. MacDonald, Proceedings of the National Academy of Sciences **108**, 12233 (2011).

[85] *See supplemental material for 1) details of the free-energy model and the relaxation problem, 2) estimation of $\mathscr{G}$ and disorder correlation functions, and 3) a microscopic expression of τ^{-1}.*

[86] F. Guinea and N. R. Walet, Phys. Rev. B **99**, 205134 (2019).

[87] S. Carr, S. Fang, Z. Zhu, and E. Kaxiras, Phys. Rev. Res. **1**, 013001 (2019).

[88] M. Koshino and N. N. T. Nam, Phys. Rev. B **101**, 195425 (2020).

[89] B. Mortazavi, M. Silani, E. V. Podryabinkin, T. Rabczuk, X. Zhuang, and A. V. Shapeev, Adv. Mater. **33**, 21022807 (2021).

[90] K. V. Zakharchenko, M. I. Katsnelson, and A. Fasolino, Phys. Rev. Lett. **102**, 046808 (2009).

[91] S. Carr, D. Massatt, S. B. Torrisi, P. Cazeaux, M. Luskin, and E. Kaxiras, Phys. Rev. B **98**, 224102 (2018).

[92] Y. Imry and S.-k. Ma, Phys. Rev. Lett. **35**, 1399 (1975).

[93] H. Fukuyama and P. A. Lee, Phys. Rev. B **17**, 535 (1978).

[94] D. Forster, *Hydrodynamic Fluctuations, Broken Symmetry, and Correlation Functions* (CRC Press, Boca Raton, 2019).

[95] A. Cano and A. P. Levanyuk, Phys. Rev. Lett. **93**, 245902 (2004).

[96] M. Baggioli and A. Zaccone, Int. J. Mod. Phys. B **35**, 2130002 (2021).

[97] Z. Bi, N. F. Q. Yuan, and L. Fu, Phys. Rev. B **100**, 035448 (2019).

[98] I. Yudhistira, N. Chakraborty, G. Sharma, D. Y. H. Ho, E. Laksono, O. P. Sushkov, G. Vignale, and S. Adam, Phys. Rev. B **99**, 140302(R) (2019).

[99] H. Ishizuka, A. Fahimniya, F. Guinea, and L. Levitov, arXiv:2011.01701 (2020).

[100] C. Rubio-Verdú, S. Turkel, L. Song, L. Klebl, R. Samajdar, M. S. Scheurer, J. W. Venderbos, K. Watanabe, T. Taniguchi, H. Ochoa, *et al.*, arXiv:2009.11645 (2020).